THE INFLUENCE OF NOZZLE SHAPE ON THE SHOCK STRUCTURE IN SEPARATED FLOWS

Francesco Nasuti, Marcello Onofri, and Elisa Pietropaoli

Dipartimento di Meccanica e Aeronautica, Università di Roma "La Sapienza", 00184 Roma, Italy

ABSTRACT

The performance of liquid rocket engines is presently limited by the side loads that take place during the startup because of the coupling between the natural flow asymmetry and a peculiar shock structure inside the nozzle. The shock and flow structures of highly overexpandend nozzles are examined numerically, with a critical discussion on the reasons yielding the different possible configurations. The results confirm that a major role is played by the flow gradients ahead of the shock and thus by the nozzle geometry.

Key words: Nozzle; Flow separation; Mach reflection.

1. INTRODUCTION

One of the possible improvements for the main engines of launchers is the development of supersonic nozzles with large area ratio, which provide higher specific impulse at high altitude with a consequent saving of a large amount of propellant. Unfortunately, large area ratio nozzles cannot be easily adopted. The reason is that the engine must be ignited at sea-level and then it has to operate from sea-level to vacuum. This aspect implies that the nozzle operates in overexpanded conditions for a long time, including the startup transient and the first phase of flight. In particular, the highly-overexpanded operation of conventional supersonic nozzles occurring during startup, usually lasting several seconds, yields flow separation that is not easily controlled and, because of the inevitable flow asymmetries, may yield unpredictable side loads even capable of leading to the nozzle structure failure.

Experimental and numerical studies have led to the common understanding that the highest side loads take place in nozzles of a particular shape, the so-called thrust optimized nozzles (Kwan and Stark, 2002; Hagemann et al, 2002), where two different separated flow structures have been found. The first flow structure, occurring at high overexpansion regime, is the classical nozzle flow separation, also referred to as free-shock separation (FSS, see Fig. 1a) by Nave and Coffey (1973). The second flow structure is more complicated (see the schematic of Fig. 1b) and shows both flow separation and reattachement with a little separation bubble. It has been referred to as restricted-shock separation (RSS) (Nave and Coffey, 1973).

In case of FSS the boundary layer separates from wall because of the adverse pressure gradient. The corresponding change of direction of the supersonic flow and the pressure rise to the ambient value, is provided by an oblique shock starting from the separation location S (Fig. 1a). Downstream, the Mach reflection of the oblique shock (ST) at the axis of the axisymmetric nozzle displays the classical shape: a nearly flat Mach stem (RT) and an oblique reflected branch.

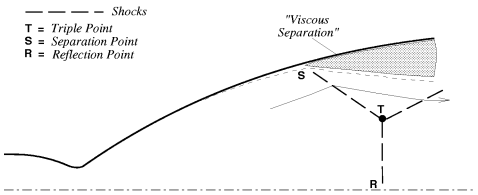

(a) Free-Shock Separation

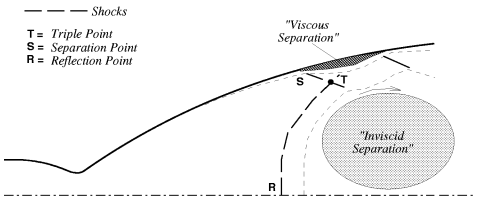

(b) Restricted-Shock Separation

Figure 1. Different kinds of Mach reflection in nozzles.

The much peculiar case of RSS has been claimed to take place in a certain range of nozzle pressure ratio (PR) and for particular nozzle profiles (Hagemann et al, 2002). Its typical structure features a large curved stem TR, also referred to as "cap-shock", and a restricted separated zone, followed by reattachment of the jet on the nozzle wall. It has been shown that in case of RSS the curved Mach stem generates a vortex behind it. The occurrence of this vortex was first shown numerically (Chen et al, 1994; Nasuti and Onofri, 1996, 1998) and later confirmed experimentally by Stark et al (2002). Nasuti and Onofri attributed the origin of this vortex to the flow nonuniformity ahead of the shock, that yields a curved shock shape and thus a rotational flow behind it (Nasuti and Onofri, 1996, 1998; Onofri et al, 1998). To distinguish the generation of the centerline vortex from that of the wall vortex generated by the boundary layer separation (i.e. "viscous separation"), the former was referred to as "inviscid separation" (Fig. 1b). Further studies (Hagemann et al, 2002) have stressed the role of the internal shock that takes place in parabolic and thrust optimized nozzles, on the bending of the Mach stem and thus on the vortex generation and RSS. The internal shock is the oblique shock that origi-

Proceedings of the Fifth European Symposium on Aerothermodynamics for Space Vehicles, 8-11 November 2005, Cologne, Germany (ESA SP-563, February 2005)

nates in these nozzles just downstream of throat and that, for a certain range of PR, impinges on the Mach stem. However, experimental tests have shown that the "inviscid separation" and possibly RSS may take place also in case of truncated ideal nozzles, where no shock impinges on the Mach stem (Kwan and Stark, 2002). As a consequence, the attention was moved again toward the role played by radial flow gradients rather than on the internal shock. Accordingly, the internal shock can be considered as one possible case of radial flow gradient, and in particular the case with the strongest gradient yielding therefore the maximum effect on the Mach stem.

The practical importance of the study of the above flow structures is due to the finding that the strongest side loads take place when the flow separation structure changes from RSS to FSS or vice versa (Frey and Hagemann, 1999). However, despite a few explanations given for the flow features yielding one or the other flow structure, further studies are needed to better understand which nozzle design can actually improve its startup behavior and why.

The present study is motivated by the above uncertainties. It aims to analyze numerically the possible flow structures in overexpanded nozzles, starting from a basic study of Mach reflections in the case of nonuniform flow ahead of the Mach stem. Subsequently the behavior of the Mach reflection depending on the particular nozzle shape considered is also discussed. The numerical simulations have been performed by using the commercial CFD software package CFD++ developed by Metacomp Technologies, Inc..

2. THE EFFECT OF UPSTREAM FLOW ON MACH REFLECTION

The basic shock-separation structure in nozzle flows is the FSS, which is a classical Mach reflection. Thus the first step to understand the possible occurrence of different flow structures is to study the reasons that could yield changes to the classical Mach reflection. To this goal it is observed that the difference between the shock reflection in a nozzle with separated flow and the theoretical Mach reflection is basically the presence of upstream radial gradients, say the upstream flow nonuniformity.

The role of upstream nonuniformity is studied by an inviscid test, which displays the behavior of the inviscid core in case of flow separation. In particular, the cross section AB (see Fig. 2) can be considered as representative of the nozzle cross section at the separation point and the quiescent ambient as representative of the separated flow region. Thus, pressure in the quiescent ambient is higher than the exhaust average pressure and its value is taken according to the experimental values reported by Ostlund (2002) for the S6 nozzle. The S6 is a cold-flow nozzle (with ratio of specific heats $\gamma = 1.4$) whose profile is a truncated ideal contour (TIC). In particular, assuming the flow conditions for nozzle pressure ratio PR=20, flow separation takes place at the cross section AB, where the

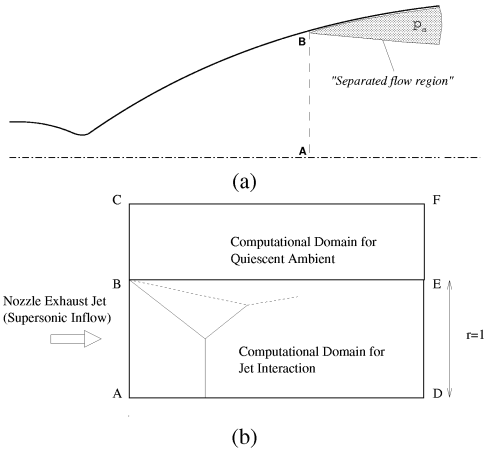

Figure 2. Test case to evaluate flow nonuniformity role on Mach reflection.

average Mach number is $M = 3.75$ (one-dimensional solution). Of course, the two-dimensional inviscid solution for the S6 nozzle at the cross section AB shows a radial gradient (Fig. 3). Based on the above values, the ambient pressure is about 5.4 times higher than the average value of the jet entering AB.

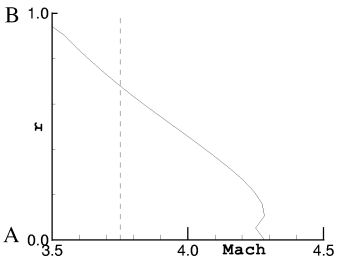

Figure 3. Uniform and TIC nozzle radial profile of Mach number at section AB.

Figure 4 shows the comparison of the following two cases: *1)* uniform flow, and *2)* flow conditions at section AB for the TIC nozzle S6. The flowfields show that the flow nonuniformity yields two important consequences: *i)* because of the increasing pressure from centerline to the wall (corresponding to decreasing Mach number at the inflow from A to B in Fig. 3), the oblique shock generated by the interaction with the ambient starts weaker in B; *ii)* the Mach stem presents a curved profile.

Indeed, if it is assumed for the sake of simplicity that the pressure in the subsonic region behind the shock is constant, it can be easily inferred that the shock intensity cannot be constant because of the upstream radial pressure gradient. The radial variation of shock intensity is provided by the increasing shock curvature, which will therefore increase for increasing upstream radial pressure gradients. It is interesting to note that the curved Mach stem is quite similar to that shown in the RSS of highly overexpanded parabolic nozzles (Nasuti and Onofri, 1996; Frey

and Hagemann, 1999). Note also that the vortex that takes place behind the curved Mach stem acts as an obstruction for the exhaust jet that is turned away from the centerline. The consequence is the larger height of the plume in the nonuniform case.

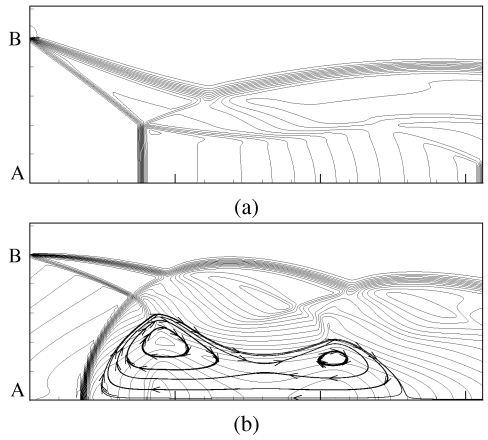

Figure 4. Mach isolines and closed streamlines for: (a) uniform supersonic inflow, and (b) nonuniform flow (TIC nozzle flow).

The numerical results shown in Fig. 4 have been confirmed by repeating the same simulation with different grid resolutions. Although the numerical viscosity rules the balance between the momentum exchange at the mixing layer and the dissipation inside the vortex, and thus grid convergence cannot be achieved for this kind of problem unless a very large number of cells is considered, very similar solutions have been obtained by doubling and quadrupling the number of cells in each direction. The results obtained by 1200, 4800, and 19200 cells, respectively, are shown in Fig. 5. The main features provided by the analysis of the flowfield have been extracted for a better comparison in Fig. 5d. It can be noticed that even at the coarsest grid level the vortex is generated, although a clear curved shape of the Mach stem cannot be detected. The second and third level show qualitatively similar solutions, however the curved shape of the shock is better resolved in the case of finest grid, and the vortical region is slightly enlarged.

3. VISCOUS OR INVISCID PHENOMENON?

Although the inviscid analysis is sufficient to explain that the "inviscid vortex" is generated by the shock curvature due to upstream flow gradients, the actual pressure level behind the shock depends on the momentum exchange in the mixing layer between the supersonic stream and the recirculating region, and on the dissipation inside the bubble. Therefore viscosity plays an important role in establishing the balance which determines the exact pressure level behind the shock, its position, dimension and position of the vortex, and the velocities inside the bubble.

To better understand this role, a series of viscous laminar computations has been carried out for the same test discussed in the foregoing section, in case of nonuniform flow (S6 nozzle with PR=20). Figure 6 shows the viscous solution computed at the full scale value of Reynolds number ($Re = 2.1 \cdot 10^6$, based on the flow values and nozzle diameter at AB). It can be seen that the solution is quite similar to that of Fig. 5. To confirm the similarity between inviscid and viscous solutions, finer and finer grids have been considered. However, to get grid-independent solutions a lower value of Re is considered which permits to manage the study with a more practical computational time. In particular, four grid levels are considered for the case with $Re = 2.1 \cdot 10^3$. The first three grid levels provide solutions qualitatively similar to the case of $Re = 2.1 \cdot 10^6$ (see Fig. 7a). Nevertheless, the finest grid shows the existence of a small normal shock between the incident shock and the curved Mach stem (Fig 7b). A possible way of evaluating the quality of the numerical solution in case of laminar flow with a vortex is to verify that the value of vorticity (ω) in case of planar flow (or its ratio to distance from the axis (ω/r) in case of axisymmetric flow) is constant (Paciorri, 1998).

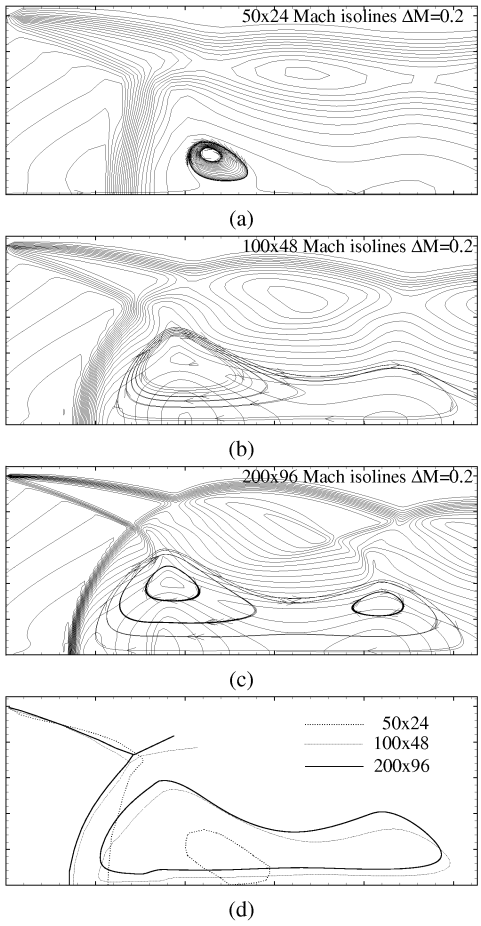

Figure 5. Grid convergence analysis for nonuniform inviscid flow: (a-c) Mach isolines and closed streamlines; (d) comparison of shock and vortex-boundary positions.

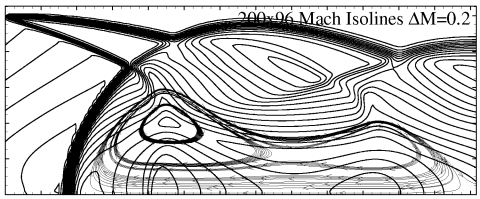

Figure 6. Mach isolines and closed streamlines for nonuniform supersonic inflow (TIC nozzle flow): viscous laminar flow with $Re = 2.1 \cdot 10^6$ (200x96 cells).

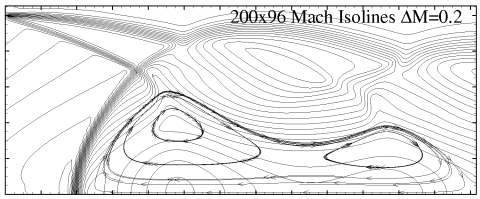

(a) 200x96 cells

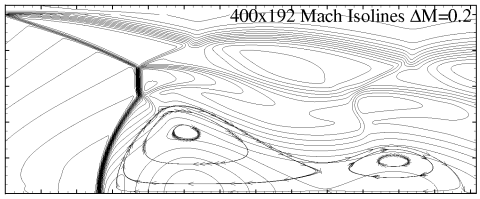

(b) 400x192 cells

Figure 7. Mach isolines and closed streamlines for nonuniform supersonic inflow (TIC nozzle flow): viscous laminar flow with $Re = 2.1 \cdot 10^3$.

This condition has been demonstrated for $Re \to \infty$ and is practically verified for values of Re large enough. In the present case, the computed behavior of ω/r as a function of the distance from the axis is shown in Fig 8a. It can be seen that the coarsest grid does not show any region of constant ω/r, whereas its behavior becomes flatter and flatter when resolution increases, indicating that the solution obtained with the finest grid is close to grid independence.

A further indication of the quality of solution is provided by the analysis of the supersonic regions (Fig. 8b). Indeed, this analysis permits to compare the position of the strong-shock branches and the existence of supersonic backflow in the bubble. Figure 8b shows that at the finest grid level no supersonic backflow takes place, as expected. As regards to the strong-shock branch, identified by the sonic line, a nonmonotonic behavior is obtained. However, the change of position between the solutions obtained by the two finer grids is due to the appearance of the small normal branch provided by the highest resolution of the shock interaction.

In conclusion, the fourth grid level considered in the low-Re case still shows a change of the solution indicating that, as in the inviscid case, a huge number of cells is needed to get a grid-independent solution. Nevertheless,

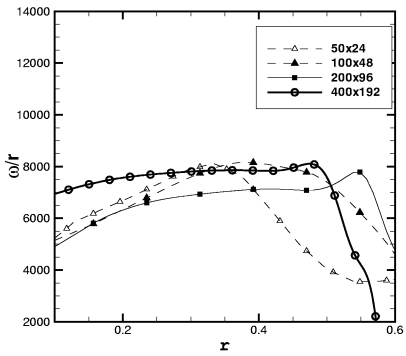

(a) Vorticity/radius ratio inside the vortex bubble

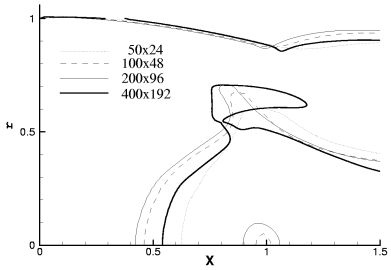

(b) Unity Mach number isoline

Figure 8. Comparison of laminar viscous solutions ($Re = 2.1 \cdot 10^3$) of nonuniform supersonic inflow test case (TIC nozzle flow) obtained with three different grid levels.

the above analysis has shown that dramatic changes of the solution cannot be expected, and that the solution qualitatively shows a flow structure quite similar to the inviscid case. Thus, it can be stressed again that the origin of the peculiar Mach reflection structure with a curved Mach stem and a vortex behind it, is of inviscid nature, in the sense that it can be predicted by the inviscid analysis.

4. THE ROLE OF TURBULENCE

After the above considerations on the role of molecular viscosity, which substantially confirms the inviscid results, it is mandatory to examine also the role of turbulence. Turbulence is taken into account by the realizable $k-\epsilon$ two-equation model for Reynolds averaged Navier-Stokes equations (Goldberg et al, 1998).

The test case of the foregoing sections is carried out again for the case of nonuniform supersonic inflow taken from the inviscid solution of S6 nozzle flowfield at the cross section AB. A sensitivity test to the turbulent flow initialization parameters has been carried out first, showing that changing their values in the admissible range does not yield strong consequences on the solution. In particular, the computations indicate that there is practically no effect of the choice of the reference turbulence length. On the contrary there is a non-negligible effect of the inflow turbulence intensity (Fig. 9). In particular, an increase

of the turbulence intensity (that is the ratio of the root-mean-square of the velocity fluctuations to the mean flow velocity) in the admissible range, reduces the bubble dimension and the shock curvature. The sonic lines show the downstream displacement of the Mach stem, while also closed streamlines move downstream. However, the role of the upstream turbulence intensity can be considered as a minor effect: the computed flow structure is not affected.

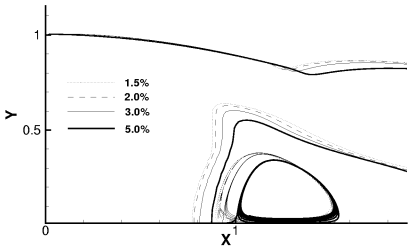

Figure 9. Mach=1 isoline and closed streamlines for different values of the inflow turbulence intensity; nonuniform supersonic inflow (TIC nozzle flow, 200x96 cells).

Considering the smallest turbulence intensity value, the computations have been then carried out for three different grid levels. The computed solutions (Fig. 10) show that most of the relevant features are captured with the coarsest grid level (19200 cells). It is important to note that unlike the cases of inviscid and viscous laminar computations, only slight changes are provided by increasing the grid resolution.

Compared to the inviscid and viscous laminar solutions, the turbulent one shows a flatter Mach stem and a smaller bubble, while the general structure (curved Mach stem and vortex behind it) is similar: the solution still shows a lower branch of the stem, whose curvature generates a big "inviscid vortex". The explanation for the smaller dimension of the vortex and for the lower velocity inside the bubble with respect to laminar computations can rely on the large effective viscosity of the turbulent flow inside the bubble.

As regards to the expected behavior in nozzles with separated flow, it is important to note that the reduced bubble dimension yields a lower upstream momentum for the flow circumventing the bubble, compared to the inviscid and laminar computations. This is an important issue to be considered when the attention is focused on the risk of flow reattachment in nozzles, because the occurrence of a curved Mach stem with a vortex behind gives rise to a "RSS-like" flow structure, which is not sufficient to lead to flow reattachment, that is to RSS. In fact, only in case of high upstream momentum for the flow circumventing the bubble, the "RSS-like" flow structure gives rise to RSS.

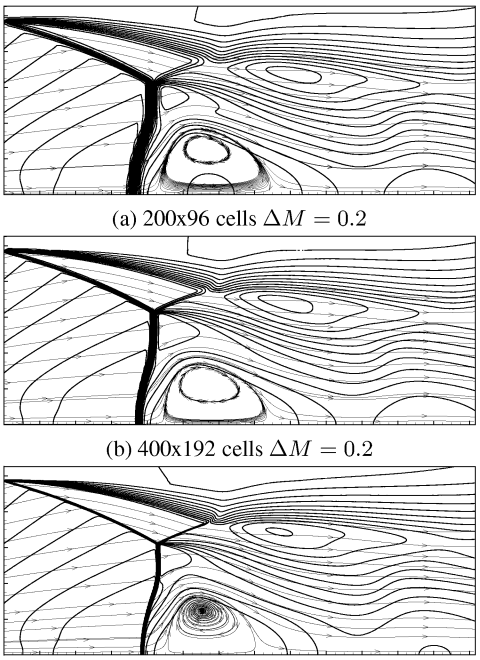

(a) 200x96 cells $\Delta M = 0.2$

(b) 400x192 cells $\Delta M = 0.2$

(c) 800x384 cells $\Delta M = 0.2$

Figure 10. Mach isolines and streamlines for nonuniform supersonic inflow (TIC nozzle flow): turbulent flow.

5. DIFFERENT FLOW NONUNIFORMITIES

After having demonstrated that the RSS-like flow structure can be generated by a typical nozzle flow gradient in radial direction, it has to be stressed that the appearance of such flow structure is connected to the strength of the radial gradients. As shown in Fig. 11 if the inflow nonuniformities are those of the same TIC nozzle but at a different pressure ratio, the vortex predicted by inviscid computation can occur or not, depending on the strength of radial gradient upstream of the shock.

In particular, it can be seen that at low pressure ratio the separation point and thus the shock system are close to the throat and the flow entering the Mach stem is quite uniform, as shown by the vertical part of the Mach isolines (Fig. 11a). As a consequence no vortex appears and slight nonuniformity yields only an upstream curvature of streamlines. In the range between PR=17 and PR=35 oblique Mach isolines impinge on the Mach stem indicating a radial gradient. The consequence is the formation of the vortex (Fig. 11b-d). Finally at the largest PR, the flow entering the Mach stem is uniform and thus the vortex disappears and streamlines are only slightly bent upstream.

6. CONCLUSIONS

The numerical study of the effects of upstream nonuniformities on a classical Mach reflection, has shown that the occurrence of radial flow gradients of the same kind

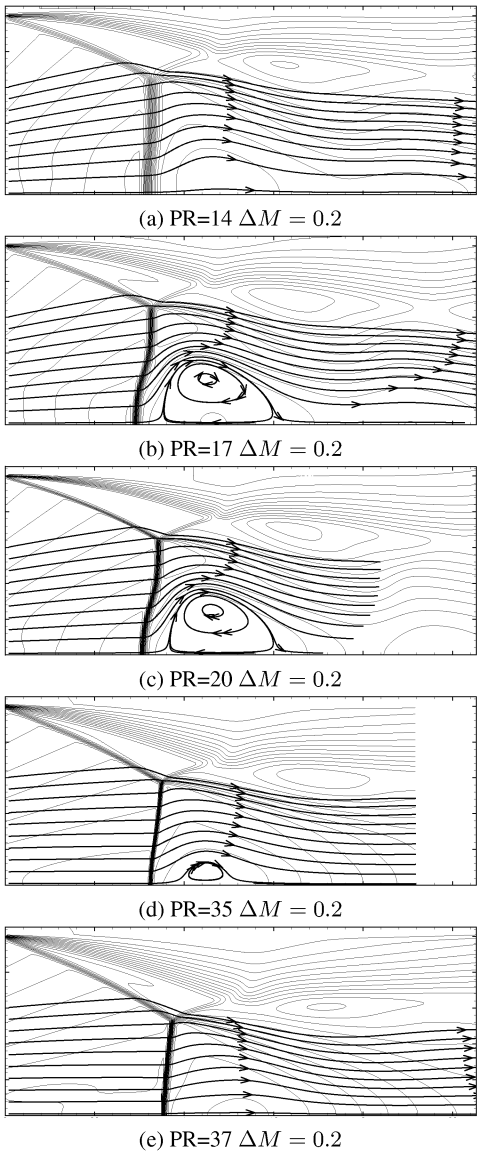

(a) PR=14 $\Delta M = 0.2$

(b) PR=17 $\Delta M = 0.2$

(c) PR=20 $\Delta M = 0.2$

(d) PR=35 $\Delta M = 0.2$

(e) PR=37 $\Delta M = 0.2$

Figure 11. Mach isolines and streamlines for nonuniform supersonic inflow (TIC nozzle flow): turbulent flow.

of those generated by a truncated ideal nozzle is sufficient to yield a strong curvature of the Mach stem. The birth of such flow structure comes from the above phenomena and is thus evidently shown by inviscid computations. The viscous laminar and turbulent computations have shown that viscosity and especially turbulence define the actual solution of the flowfield, however the phenomena predicted by the inviscid simulation are smoothed, not cancelled, by the viscous effects.

The numerical demonstration of the reasons leading to the existence of a "RSS-like" flow structure, could help to design possible improvements of nozzle geometries. However, the operating conditions leading to transition from "RSS-like" to RSS flow structure have to be still investigated in detail and that should represent a mandatory analysis to be performed in the future studies.

7. ACKNOWLEDGEMENTS

This work was partially sponsored by Italian Ministry for Education University and Research (MIUR).

REFERENCES

Chen, C., Chakravarthy, S., and Hung, C. Numerical investigation of separated nozzle flows. *AIAA Journal*, 32(9):1836–1843, September 1994.

Frey, M. and Hagemann, G. Flow separation and side loads in rocket nozzles. AIAA Paper 99–2815, July 1999. 35th AIAA/ASME/SAE/ASEE Joint Propulsion Conference.

Goldberg, U., Peroomian, O., and Chakravarthy, S. A wall-distance-free k-e model with enhanced near-wall treatment. *Journal of Fluids Engineering*, 120(3):457–462, September 1998.

Hagemann, G., Frey, M., and Koschel, W. Appearance of restricted shock separation in rocket nozzles. *Journal of Propulsion and Power*, 18(3):577–584, May-Jun 2002.

Kwan, W. and Stark, R. Flow separation phenomena in subscale rocket nozzles, July 2002. 38th AIAA/ASME/SAE/ASEE Joint Propulsion Conference and Exhibit, Indianapolis, Indiana.

Nasuti, F. and Onofri, M. Viscous and inviscid vortex generation during nozzle flow transients. AIAA Paper 96–0076, January 1996. 34th AIAA Aerospace Sciences Meeting & Exhibit.

Nasuti, F. and Onofri, M. Viscous and inviscid vortex generation during start-up of rocket nozzles. *AIAA Journal*, 36(5):809–815, May 1998.

Nave, L. and Coffey, G. Sea level side loads in high-area-ratio rocket engines. AIAA Paper 73–1284, November 1973. 9th AIAA/SAE Propulsion Conference.

Onofri, M., Nasuti, F., and Bongiorno, M. Shock generated vortices and pressure fluctuations in propulsive nozzles. AIAA Paper 98–0777, January 1998. 36th AIAA Aerospace Sciences Meeting & Exhibit.

Östlund, J. *Flow processes in rocket engine nozzles with focus on flow separation and side loads*. Licentiate Thesis, Royal Institute of Technology Department of Mechanics, Stockholm, Sweden, 2002.

Paciorri, R., Sabetta, F., and Favini, B. On the numerical solution of recirculating bubbles at large reynolds number. AIAA Paper 98–2813, June 1998. 29th AIAA Fluid Dynamics Conference.

Stark, R., Kwan, W., Quessard, F., Hagemann, G., and Terhardt, M. Rocket nozzle cold-gas test campaigns for plume investigations. In *Proceedings of the 4th European Symposium on Aerothermodynamics for Space Vehicles, 15th-18th October 2001*, pages 611–618, ESA SP-487, Noordwijk, The Netherlands, March 2002. ESTEC.